PAUL SCHERRER INSTITUT

REM continuation
Change of contract 11108/94/NL/JG(SC)

Technical note on WP 81

P. Bühler, W. Hajdas, A. Zehnder

PSI, May 1998
Version 1.0

Contents

1 Purpose

The purpose of this document is threefold:

- identify the potential power of SREM to resolve the energy spectra of protons and electrons
- discuss data analysis methods
- make requirements for detector simulations

The result of an SREM measurement is the number of detected counts in fifteen counters, a fifteen channel histogram. From this limited information we hope to extract information on the energy spectra of the detected particles, the particle species, and probably also on the angle of incidence.

The following investigation is based on simulations of the SREM carried out in winter 1996/1997 at PSI [*Hajdas,* 1997]. The simulations include the whole detector box, but no additional shielding by surrounding material (e.g. satellite). The applied geometry of the SREM detector was based on the technical drawings available at that time, which have slightly changed since then.

Therefor the presented results are only preliminary. Nevertheless, the main conclusions should not be affected by future studies which will be carried out with improved simulations. This analysis does not consider ions, which has to be added latter on.

2 Detector response

2.1 Simulations

For the simulations, on which this study is based, isotropic particle fluxes were assumed. The differential proton spectrum $f_p(E)$ was simulated by a powerlaw $f_p = A_p \cdot E^{-\gamma_p}$ $[cm^{-2}MeV^{-1}]$ with $\gamma_p = 2$ and the electron spectrum by an exponential function $f_e = A_e{\cdot}exp(-\gamma E)$ $[cm^{-2}MeV^{-1}]$ with $\gamma_e = 1.706$.

Per detector d_{12}, d_3, and particle species, protons and electrons, $2 \cdot 10^7$ particles were simulated, which corresponds to a 4π-fluence of $7.958 \cdot 10^5$ particles per cm^{-2} (see Appendix A) in the energy ranges described in table 1. Given the 4π-fluence in the defined energy ranges and the shape of the energy spectra, the normalizations $A_{p,e}$ can be calculated, which are also listed in table 1. In the last row the resulting number of detected events are listed. The low number of detected electrons indicates the limited statistics of this sample.

Table 1: Energy range and normalization of the simulated particle spectra.

Detector	Particles	E_{min}	E_{max}	$A_{p,e}$	n_{det}
		[MeV]		$[cm^{-2}MeV^{-1}]$	
d_{12}	p	30	300	$3.41 \cdot 10^7$	96466
d_{12}	e	0.3	6.0	$4.53 \cdot 10^6$	538
d_3	p	8	300	$1.31 \cdot 10^7$	95881
d_3	e	0.3	6.0	$4.53 \cdot 10^6$	4762

As result of the simulations, event tables were generated, containing incident energy, angle of incidence, and energy deposits in the three detectors. According to the SREM discriminator levels given in table 2 [*Vuilleumier,* 1997] these data can be sorted by the energy deposits in the three detectors, and histograms of the counts in the fifteen detector counters (TC1, S12, S13, S14, S15, TC2, S25, C1, C2, C3, C4, TC3, S32, S33, S34) can be calculated.

2.1.1 Simulating arbitrary spectra

In order to calculate count histograms for any incident spectrum, the simulated events can be weighted. Thus in order to simulate a spectrum $g(E)$, each event is given a weight

$$w = g(E) \cdot f_{p,e}(E)^{-1} \tag{1}$$

Table 2: SREM counter thresholds

number	counter	E_{th} [MeV]					
		d1		d2		d3	
		min	max	min	max	min	max
1	TC1	0.085	-	-	-	-	-
2	S12	0.25	-	-	-	-	-
3	S13	0.6	-	-	-	-	-
4	S14	2.0	-	-	-	-	-
5	S15	3.0	-	-	-	-	-
6	TC2	-	-	0.085	-	-	-
7	S25	-	-	9.0	-	-	-
8	C1	0.6	-	2.0	-	-	-
9	C2	0.6	-	1.1	2.0	-	-
10	C3	0.6	-	0.6	1.1	-	-
11	C4	0.085	0.6	0.085	0.6	-	-
12	TC3	-	-	-	-	0.085	-
13	S32	-	-	-	-	0.25	-
14	S33	-	-	-	-	0.75	-
15	S34	-	-	-	-	2.0	-

2.2 Energy response

Unlike a spectrometer which is able to measure the incident particle spectrum in narrow distinct energy intervals, SREM samples the spectra in broad, not sharply defined, and overlapping energy bands, represented by the energy response of the fifteen detector counters. The number of counts in a specific counter can not be related in a simple manner to the incident particle flux at a given energy.

The relation between the counts in counter i, c_i and the incident particle flux $f_k(E)$ is given by the following set of integral equations

$$c_i = \int_0^\infty f_k(E) \cdot G_k(E, i) dE \tag{2}$$

where $G_k(E, i)$ is the geometric factor and represents the energy response of counter i to particle species k. How these equations are used to deduce $f_k(E)$ from the measured c_i is the subject of section 3.

In the following we use relation (2) to deduce the geometric factors from the available simulations. We therefor simulate a flat spectrum $f_{p,e} = 1\ [cm^{-2}MeV^{-1}]$ with the weigthing method describe above (section 2.1.1). By differentiation of the resulting c_i with respect to E (here done by computing a histogram of the detections in counter i as function of E), $G_k(E, i)$ is obtained.

The energy response of each counter is summarized in table 2, while the simulation results are shown in figures 1 and 2 for protons and electrons, respectively. There are four (protons)/three (electrons) panels per detector counter. The upper two/one panels show contour plots of all detected events in the E-dE plane for detector d_1/d_3 (left) and d_2 (right). The vertical lines mark the counter thresholds. The lower right panels show the histograms of the number of counts as function of energy E (geometric factors). The full line represents the total number of counts, the dotted line events with an angle of incidence $\varphi < 20°$ (through aperture), and the dash-dotted line events with $\varphi > 20°$. In the lower right panels finally, histograms of the number of counts as function of angle of incidence are shown. The vertical lines mark the opening angle of the detector entrance cone of 20°.

2.2.1 Remarks

It must be kept in mind that these results represent the energy response of the standalone SREM box. Although SREM has a geometrically well defined aperture, protons penetrate from all directions. At proton energies above 80 MeV the geometric factors are even dominated by particles penetrating from outside the aperture. It can be expected that the mass of the spacecraft on which SREM will be mounted will alter this part of the energy response. Especially at $\varphi > 90°$ the energy threshold will be moved from the present ≈ 80 MeV up to higher energies. This will play a rolw when we have to define what we consider to be a particle incident from front and from back (see section 4).

In case of the coincidence counters C1, C2, C3, and C4, where detections are restricted to nearly perpendicularly incident particles the angular distribution does not show a clear cut-off at 20°. The width of the angular distribution is rather 30° to 40°.

Electrons are better confined to the aperture. But also for electrons the width of the angular distribution is $> 20°$. Note that the statistics of the electrons is poor!

In the following, some relevant features of the response functions are listed.

a) Counters S14, S15, S25, C1, C2, C3, C4, and S34 are pure proton counters.

b) There are no pure electron counters.
Counters TC1, S12, S13, TC2, TC3, S32, and S33 are sensitive to electrons.

c) Counter S15 measures practically neither protons nor electrons and can be used to measure cosmic ions.

d) Counter S25 which was hoped to measure only cosmics, can be contaminated by protons with angles of incidence $\varphi \approx 90°$.

e) Protons with energies above 80 MeV penetrate the detector from 4π. With the satellite as additional shielding this energy threshold will be increased.

f) Counters TC1 and S12 (TC3 and S32) have the same energy response to protons. There are approximately ten counters which are sensitive to protons with significantly different response functions (complementary counters). The number of complementary counters determines the energy resolution of the instrument. The higher the number the better the resolution.

g) TC1 and TC3, S12 and S32, and S13 and S33 have a similar energy response to electrons. There are approximately four complementary electron counters.

Table 3: Characteristics of the energy response of the fifteen SREM counters

Counter	Species, in/out aperture ($\pm 20°$)	Energy range [MeV]	Comments
TC1	p, in	20 - 300	
	p, out	20 - 300	
	e, in	0.8 - 5.5	
	e, out	0.8 - 5.5	
S12	p, in	20 - 300	For protons same as TC1
	p, out	20 - 300	
	e, in	0.8 - 5.4	
	e, out	0.8 - 5.4	
S13	p, in	20 - 150	
	p, out	20 - 300	
	e, in	3.5 - 5.0	
	e, out	3.5 - 5.0	
S14	p, in	20 - 50	No electrons
	p, out	20 - 300	
	e, in	–	
	e, out	–	
S15	p, in	20 - 50	Only few protons and no electrons
	p, out	80 - 300	
	e, in	–	
	e, out	–	
TC2	p, in	40 - 300	Only highest energy electrons through aperture
	p, out	40 - 300	
	e, in	> 5	
	e, out	–	
S25	p, in	–	No protons from front (they come in from side), no electrons
	p, out	80 - 150	
	e, in	–	
	e, out	–	
C1	p, in	40 - 250	No electrons
	p, out	80 - 300	
	e, in	–	
	e, out	–	
C2	p, in	40 - 100	No electrons
	p, out	40 - 200	
	e, in	–	
	e, out	–	
C3	p, in	60 - 150	No electrons
	p, out	60 - 250	
	e, in	–	
	e, out	–	

continued on next page

continued from previous page

Counter	Species, in/out cone (±20°)	Energy range [MeV]	Comments
C4	p, in	110 - 300	No electrons
	p, out	110 - 300	
	e, in	–	
	e, out	–	
TC3	p, in	10 - 300	
	p, out	10 - 300	
	e, in	0.4 - 6.0	
	e, out	0.4 - 6.0	
S32	p, in	10 - 300	For protons same as TC3
	p, out	10 - 300	
	e, in	0.4 - 4.0	
	e, out	0.4 - 4.0	
S33	p, in	10 - 150	
	p, out	10 - 300	
	e, in	0.6 - 4.0	
	e, out	0.6 - 4.0	
S34	p, in	10 - 80	No electrons
	p, out	10 - 300	
	e, in	–	
	e, out	–	

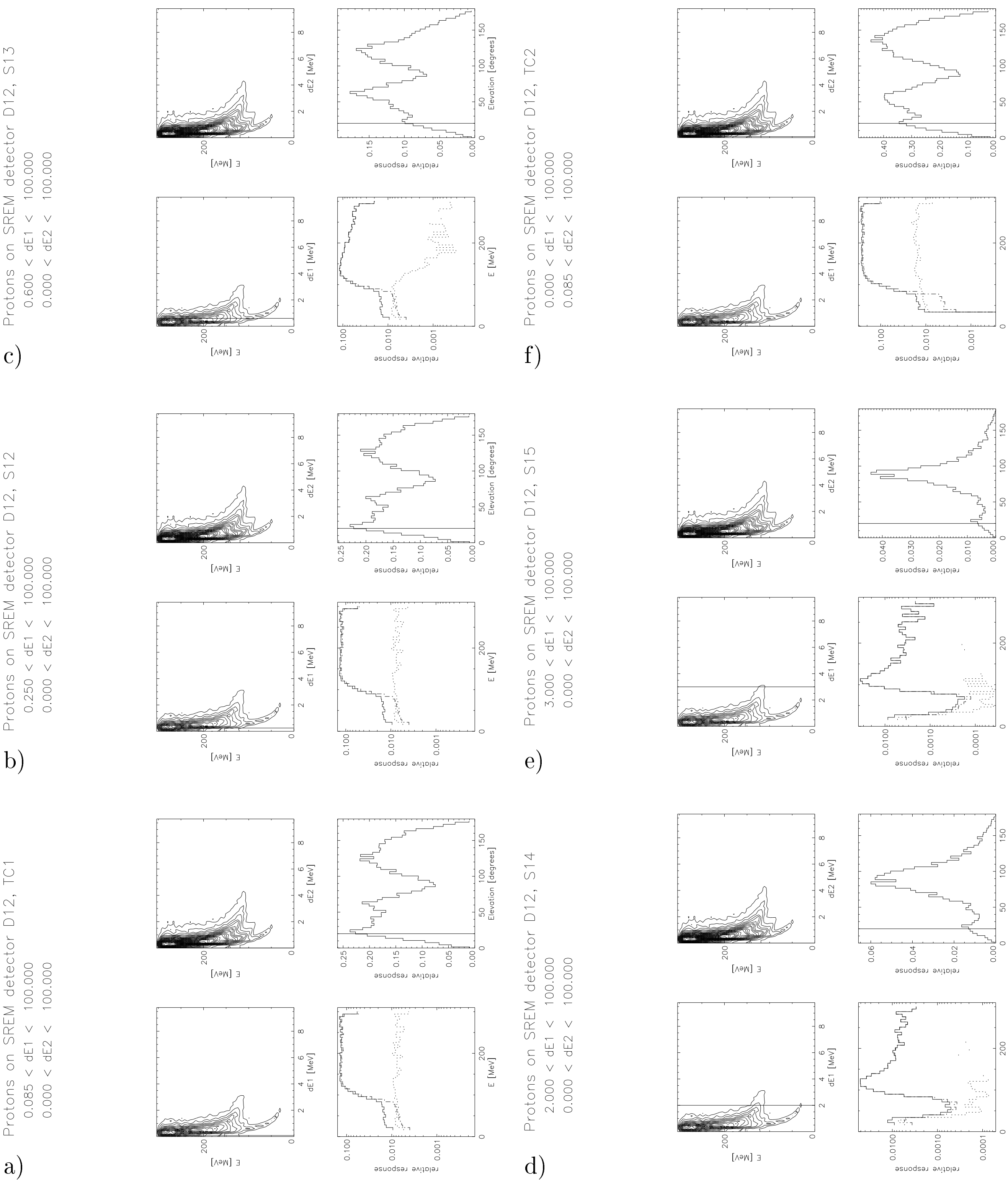

figure 1 continued on next page

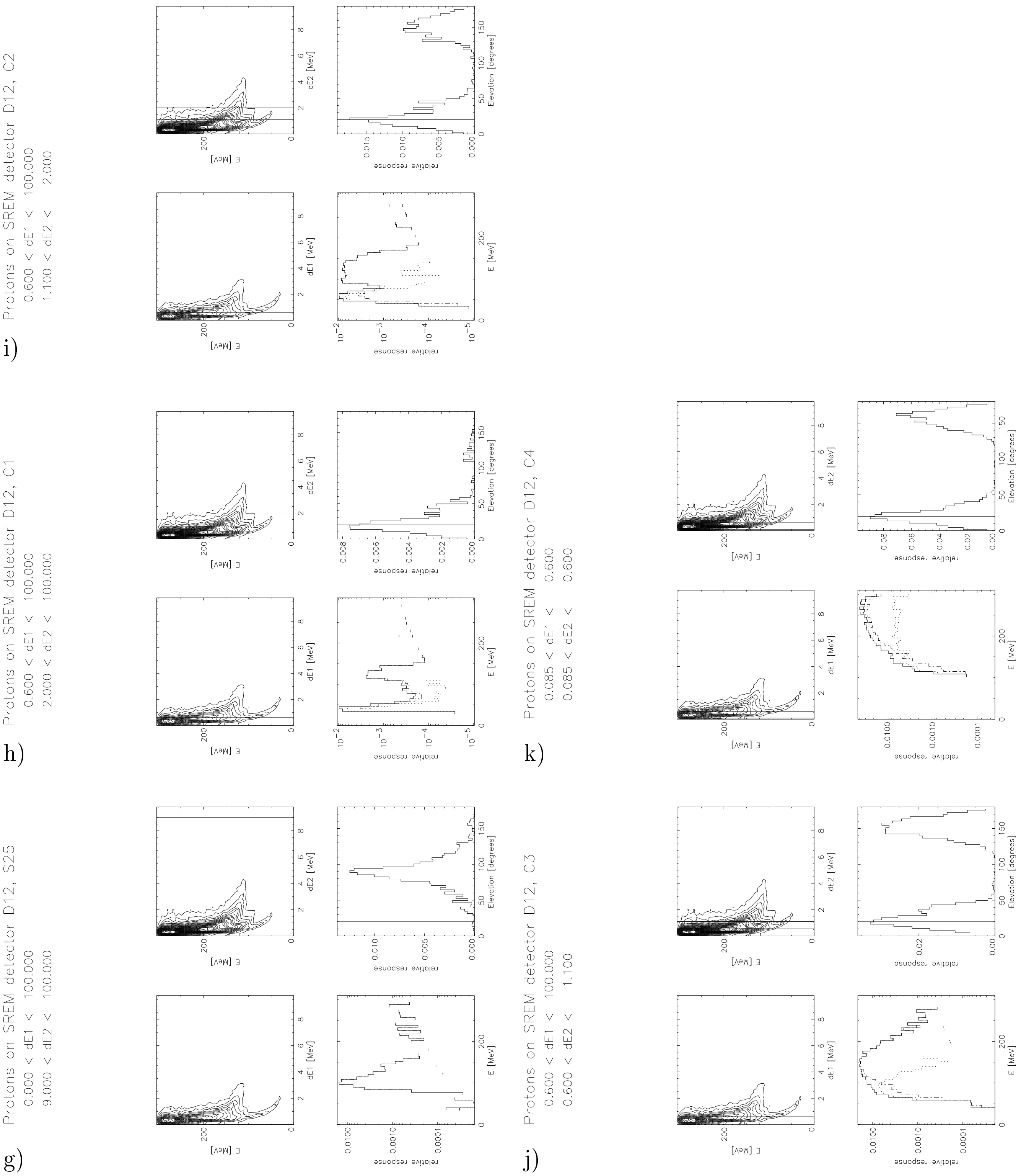

figure 1 continued on next page

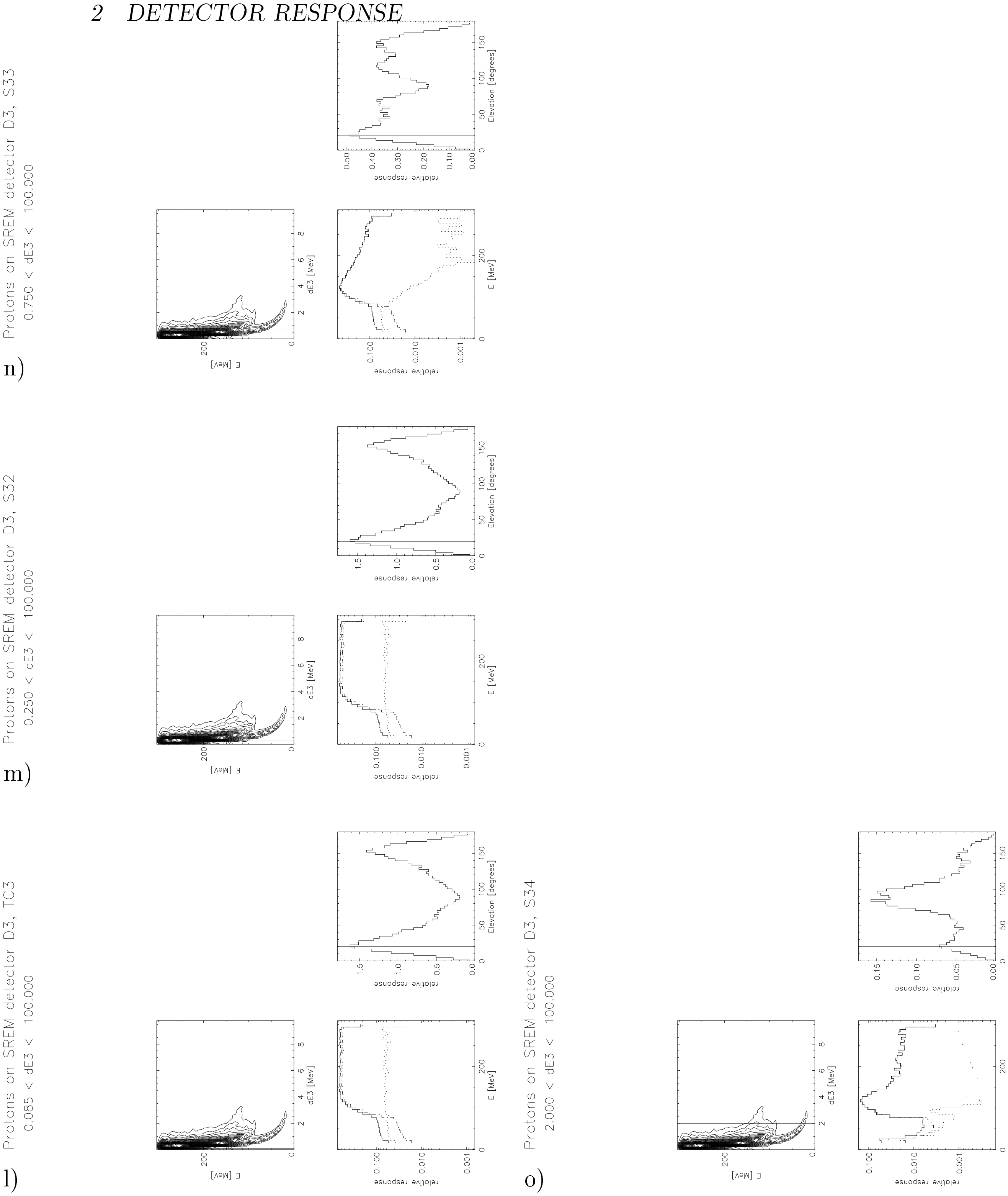

Figure 1: Energy and angular response of the fifteen SREM counters to protons in the energy range between 20 and 300 MeV. The upper two (one in case of detector 3) boxes of each panel show contour plots of the energy deposits $dE_{1,2,3}$ versus incident energy in detectors 1 and 2. The vertical lines mark the energy thresholds of the specific counter. In the lower-left boxes the number of detections are plotted as function of the incident energy (full line). The dotted line represents the particles coming through the entrance cone of $\pm 20°$, and the dash-dotted line, the particles coming from outside the entrance cone, respectively. The lower-right boxes show the number of detections as function of the angle of incidence.

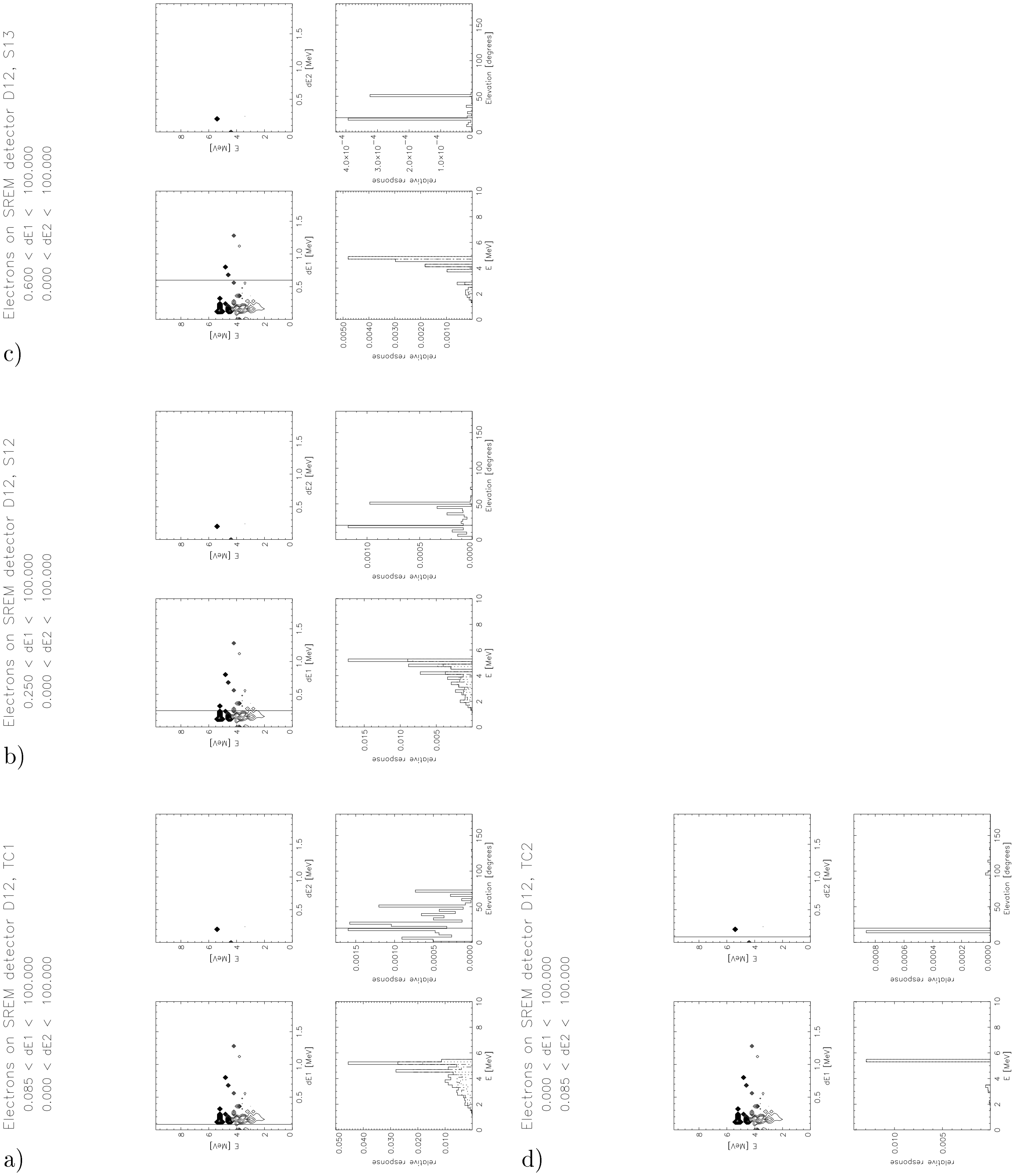

figure 2 continued on next page

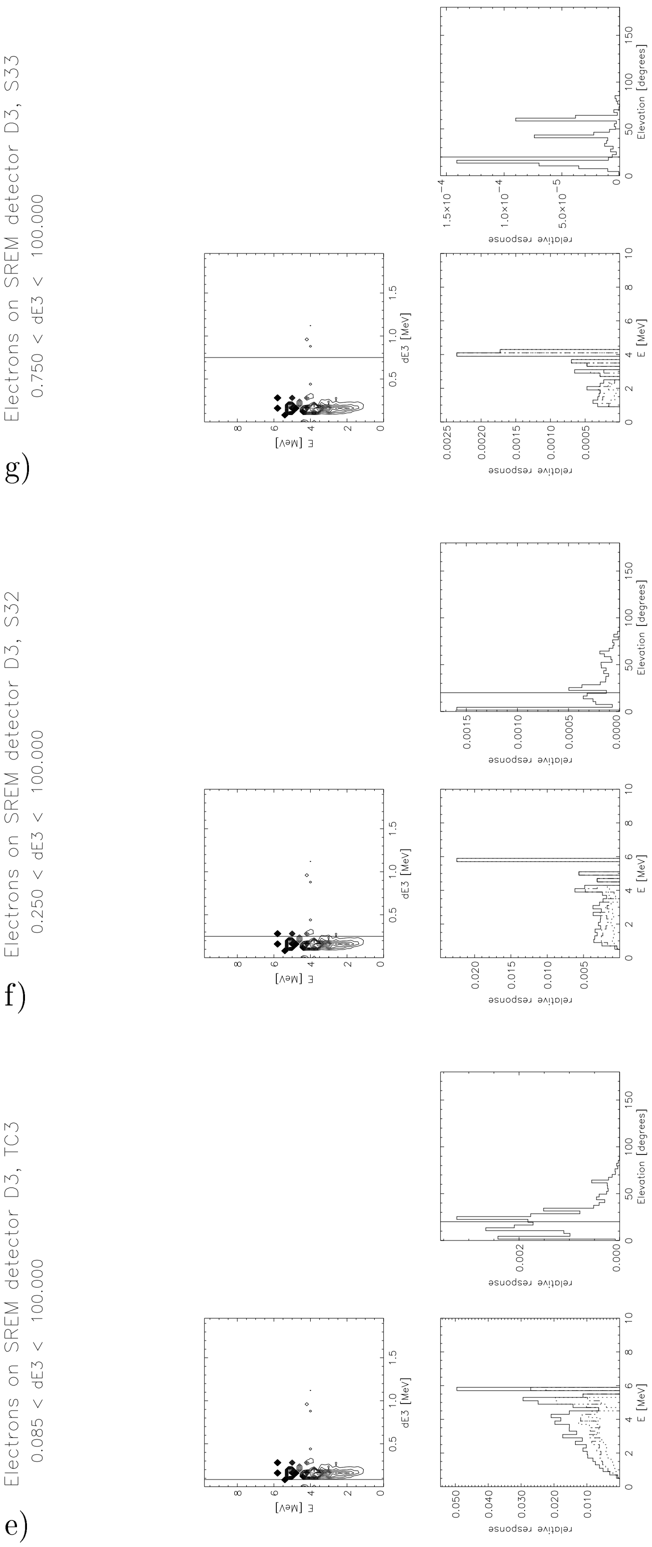

Figure 2: Same as figure 1, but for electrons in the energy range between 0.3 and 6.0 MeV. No diagrams are plotted for the counters which are not sensitive to electrons.

3 Information extraction

3.1 Deadtime correction

The deadtime $t_{D_{1,2,3}}$ of all three detectors is directly measured by SREM with the counters PL1,2,3. At the detection of an event the SREM electronics opens a gate which is closed again when the output signal goes below the TCi threshold. As long as the gate is open, no new event is accepted. SREM repeatedly (N_{check} times per second) checks whether the gate is open and counts the number of cases PLi it finds it to be open. This measurement is used to correct the counts for deadtime effect. The number of detections must be multiplied with

$$c_{i_{corr}} = c_i \cdot \frac{1}{1 - PLi/(N_{check} \cdot t_{acc})} \tag{3}$$

where t_{acc} is the accumulation time.

The length of a gate depends on the signal amplitude. The larger the signal the longer the gate time. Thus the deadtime is not only related to the count rate (TCi) but also to the signal heights, which depends on the particle species and its energy. It is therefor not possible (contrary to REM, where the gate time had a fixed length) to deduce the deadtime from the count rates alone without additional assumptions. It is possible that we learn with the real data to relate PLi with TCi.

3.2 Dose

Computing the total energy deposit in the different detectors it must be considered, that events can be contained in different counters. Equations 4 to 6 are the formula for the dose calculations. $\overline{dE_i}$ denotes an average deposited energy. The dose measure in detector d2 is rather crucial as there are only two counters without coincidences (should speek of ‘restricted dose’ here).

$$\begin{aligned}
D_{d1} &= c_5 \cdot \overline{dE_5} + (c_4 - c_5) \cdot \overline{dE_4} + (c_3 - c_4) \cdot \overline{dE_3} + \\
&\quad (c_2 - c_3) \cdot \overline{dE_2} + (c_1 - c_2) \cdot \overline{dE_1} && (4)\\
D_{d2} &= c_7 \cdot \overline{dE_7} + \\
&\quad (c_6 - c_7) \cdot \overline{dE_6} && (5)\\
D_{d3} &= c_{15} \cdot \overline{dE_{15}} + (c_{14} - c_{15}) \cdot \overline{dE_{14}} + (c_{13} - c_{14}) \cdot \overline{dE_{13}} + \\
&\quad (c_{12} - c_{13}) \cdot \overline{dE_{12}} && (6)
\end{aligned}$$

The values $\overline{dE_i}$ are not well determined but must be within ranges defined by the counter thresholds, e.g. $0.085 \leq \overline{dE_1} \leq 0.25$ MeV, $0.25 \leq \overline{dE_1} \leq 0.6$ MeV, and so on.

As an approximation the arithmetic average of the thresholds can be used, thus $\overline{dE_1}$=0.165 MeV, $\overline{dE_2}$=0.0.45 MeV, and so on. In order to get a better approximation the deposited energies are simulated for different incident particle spectra. Using the weighting method described in a previous section the detector response to these spectra is computed. Then the simulated data is used to calculate the true dose in each counter interval and by dividing these values by $(c_i - c_{i+1})$ the $\overline{dE_i}$ are found. Results of such calculations are shown in figure 3 for

a) protons, and b) electrons) where the $\overline{dE_i}$ are plotted as function of the spectral index. The full lines represent the counters of detector d1, the dotted lines the counters of detector d2, and the dash-dotted lines the counters of d3. The asterisks, diamonds, and squares mark the centre of the bins, while the error bars show the width of the counter intervals (l.t.r. counter of d1, d2, and d3). The values are rather independent of the spectral index γ, indicating that for each channel an average value can be used to calculate the total dose without knowledge of the incident particle spectrum.

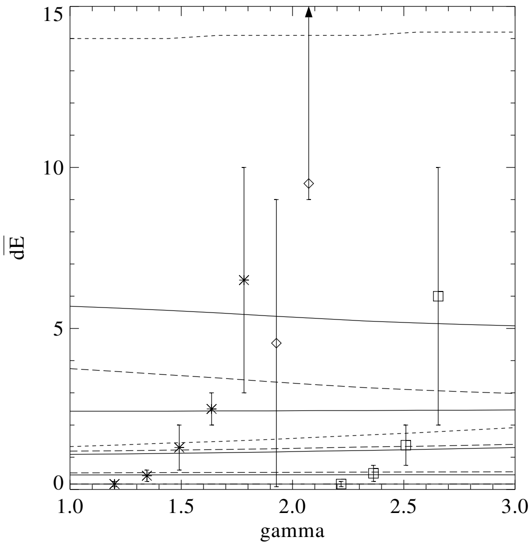

a)

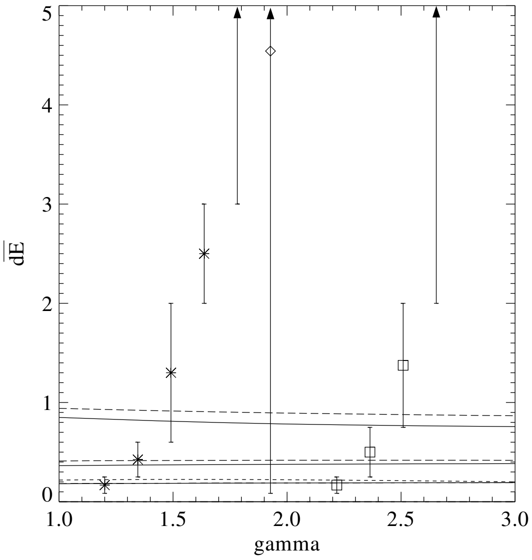

b)

Figure 3: $\overline{dE_i}$ as function of the spectral index γ for a) protons and b) electrons. The full lines represent energy deposit bins of detector d1, the short dashed lines deposit bins of detector d2, and the long dashed lines, counters of detector d3. The error bars show the width and the asteriksdiamondssquares mark the center of the bins.

3.3 Spectral information

3.3.1 Channel ratio

Count ratios between different detector counters can provide some information on the incident particle spectra. Although a ratio does not determine absolute fluxes, it can be used to specify the spectral hardness. This can be interesting for monitoring spectral variations. However, it must be noted that changes of a counter ratio can indicate either a spectral variation, a changing composition (protons, electrons, ions), a changing angular distribution, or even a modification of the detector performance, e.g. due to temperature variation.

Best suited for usage as spectral hardness indicator is a ratio of counters which only count one specific type of particle. Indeed there is a series of counters which are only sensitive to protons (see section 2.2) but no counter only sensitive to electrons.

In order to maximize the sensitivity of the ratio to spectral changes, one of the two counters used to compute the ratio should be most sensitive to the high energies and the other one to low energies. In this sense the ratios C4/C2, C4/C3, C4/S14, or C4/S34 promise to be good proton spectral hardness indicators. For electrons ratios TC1/S32, S13/S33, S13/S32, or S12/TC3 are most promising. In figure 4 the simulated ratios are plotted as function of the spectral index.

3.3.2 Spectral resolving power

The relation between the incident particle fluxes $f_k(E)$ $[s^{-1}cm^{-2}MeV^{-1}]$ and the measured counts c_i $[s^{-1}]$ is defined by the set of integral equations

$$c_i = \sum_{\text{k=species}} \int_0^\infty f_k(E) \cdot G_k(E,i) dE \tag{7}$$

where $G(E,i)$ is the geometric factor in cm^2. k denotes specific groups of particles which can contribute to the number of counted events. So, different types of particles but also for example the protons with angles of incidence $\varphi < 20°$ are possible groups. Two groups can be resolved if their geometric factors are sufficiently different.

In order to obtain the incident particle spectra from the measured count histograms equation (7) must be solved, the measured histograms must be unfolded.

Any unfolding method uses a kind of fitting. The involved spectra must be parametrized in some way and the parameters, a_l optimized in order to minimize the difference between the measured histograms and the histograms calculated with equation (7).

A reliable measure for the difference between the measured $c_{i_{mes}}$ and calculated $c_{i_{calc}}(a_l)$ histograms is χ^2, which is defined by

$$\chi^2 = \sum_i \left(\frac{(c_{i_{mes}} - c_{i_{calc}}(a_l))^2}{\sigma^2_{i_{mes}} + \sigma^2_{i_{calc}}} \right) \tag{8}$$

where the $\sigma_{i_{mes}}$, $\sigma_{i_{calc}}$ are the uncertainties of the measured and calculated counts. Note that in the case where the number of counts per bin turns out to be very low, the maximum likelihood ratio method [*Cash,* 1976],[*Cash,* 1979] may be preferable to χ^2.

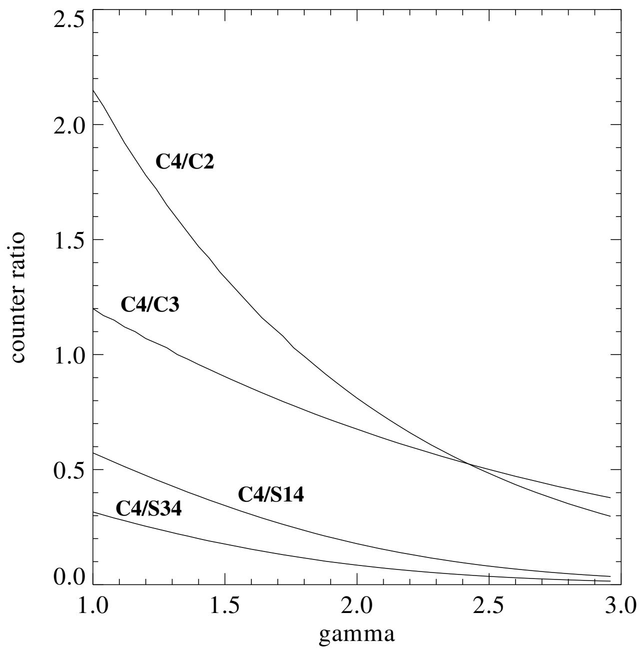

a)

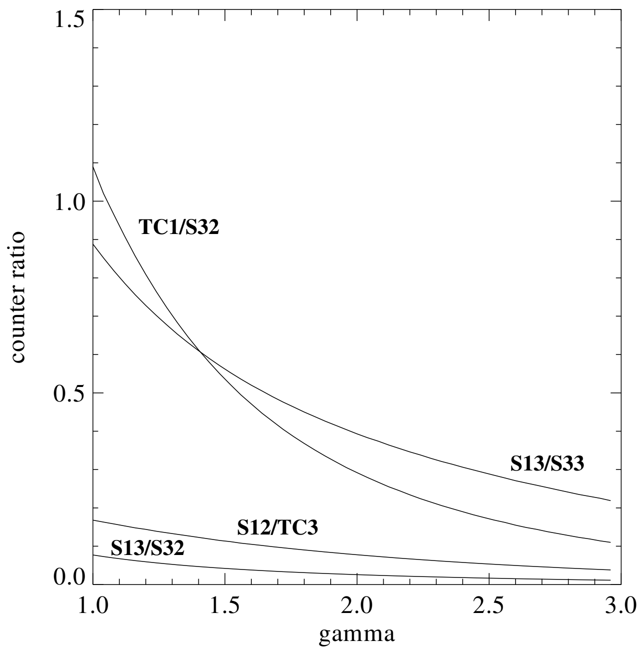

b)

Figure 4: Counter ratios as function of the spectral index γ. a) protons, counter ratios C4/C2, C4/C3, C4/S14, and C4/S34 b) electrons, counter ratios TC1/S32, S13/S33, S13/S32, and S12/TC3.

In order to estimate the spectral resolving power of SREM we calculate χ^2 as function of spectral model parameters a_l with equation (8).

As no real measurements are available, the measured histogram $c_{i_{mes}}$ is replaced by a calculated histogram with fixed parameters $a0_l$. Then the parameters are varied and for each set of parameters the $c_{i_{calc}}(a_l)$ and the corresponding χ^2 is calculated.

χ^2 as function of the model parameters has a minimum at $a_l = a0_l$ and increases with increasing distance of the model parameters from $a0_l$. According to the definition of χ^2 the uncertainty of a parameter is the range within which χ^2 increases by 1. If the function is steep, already a small deviation of the parameters from the nominal values results in a considerable increase of χ^2. Thus the steeper the increase of the function outside the minimum, the smaller the parameter uncertainty, and the better the resolution is.

For the following calculations the proton spectra were parametrized by a power law and the electron spectra, by a exponential function.

In a first series of calculations χ^2 was calculated as function of the spectral index. The spectral normalizations were selected to keep the total number of counts in the histograms constant. Figure 5 a) shows the result for protons and b), for electrons. In the presented case the initial power law index of the proton spectrum was set to γ_p=2.0 and the exponential index of the initial electron spectrum, to γ_e=1.7. The three lines represent results for different numbers of total counts (1.e3, 1.e4, 1.e5). Of course, the higher the number of counts, the better the spectral index is defined (the steeper the χ^2-curve is).

In a second series of calculations, χ^2 was determined as function of both spectral parameters, the normalization and the spectral index. In figure 6 (protons) and figure 7 (electrons) contour plots of the resulting χ^2 surfaces are plotted in the spectral index - normalization plane for different values of the total number of counts in the "measured" histograms. The three lines in each panel represent χ^2 values of 1, 5, and 10.

There are several things to note:

- The calculations represent an ideal case. They do not take into account errors of the detector response function and contain no statistical noise. Both effects would contribute to a broadening of χ^2.

- The calculations represent the specific case of a proton power law spectrum and an electron exponential spectrum.

- Pure proton or electron measurements are assumed. In reality a mixture of different types of particles is measured which will increase the uncertainty of the fitted parameters.

- Whereas the spectral index of the proton spectra are rather well defined, ±5% at 10^4 counts, the normalization has large uncertainties, ±50% at 10^4 counts. This is mostly due to the fact, that small changes of the spectral index cause large flux variations in the relevant energy range (E > 20 MeV) even if the amplitude is kept constant ($\Delta f(E_0) = A \cdot E_0^{-\Delta\gamma}$; E_0 = 50 MeV, $\Delta\gamma$ = 0.1, $\Delta f(E_0) \approx 1.5$). Because the flux around 50 MeV must be more or less constant for best fitting spectra, independent of γ, the effect is compensated by large changes of the amplitude, which represents the flux at 1 MeV (note that this effect does not appear in the electron simulations, because there the relevant energy range is around 1 MeV). Instead of the amplitude A one can also use the flux

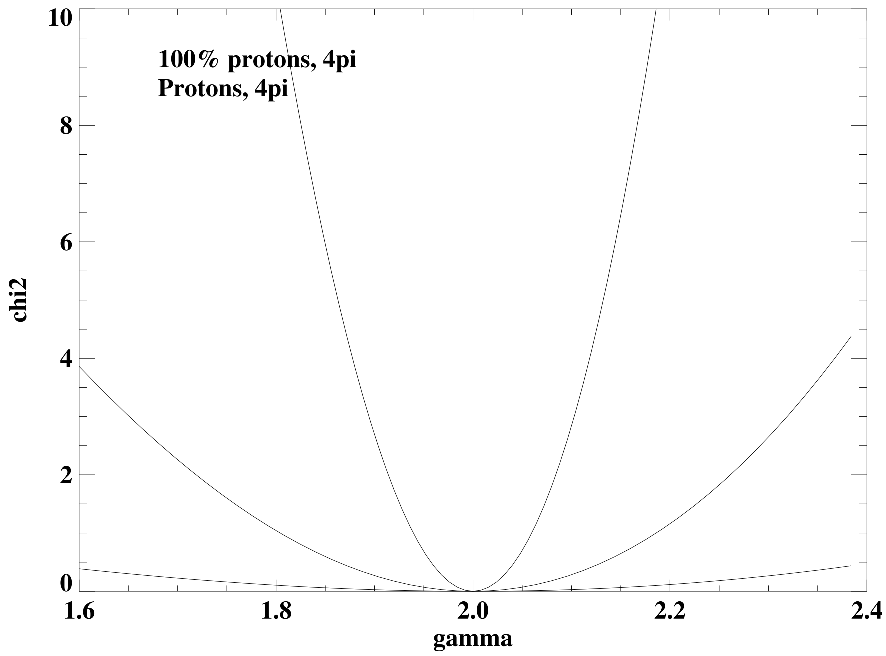

a)

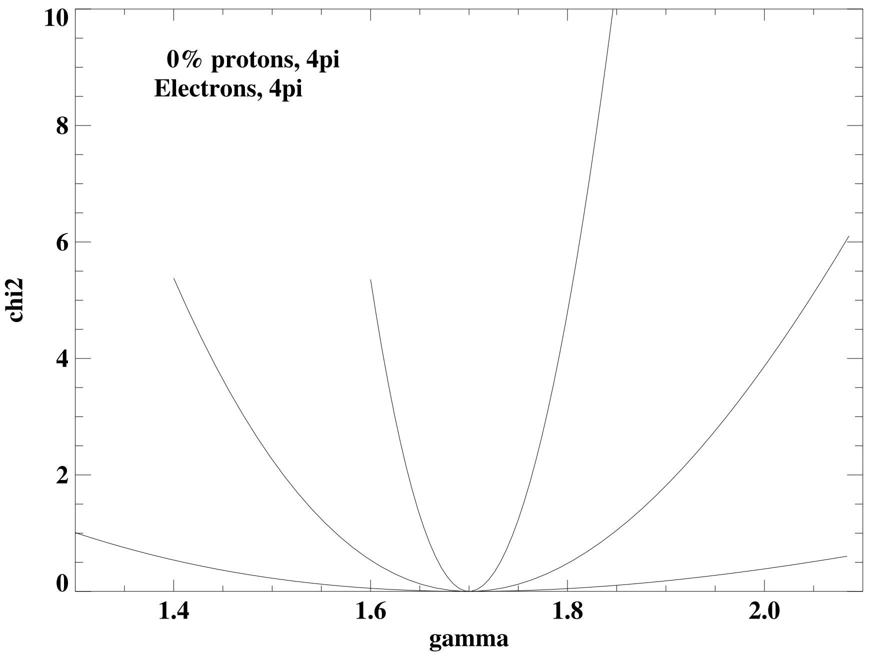

b)

Figure 5: χ^2 as function of the spectral index γ for a) protons with a power law spectrum and b) electrons with an exponential spectrum. the three lines show results for different numbers of total counts (b.t.t.) 10^3, 10^4, and 10^5.

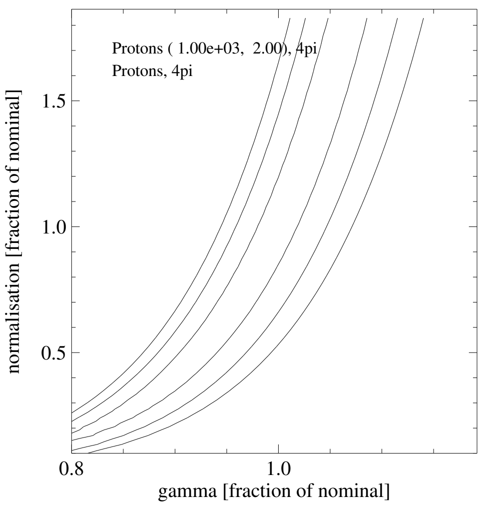

a)

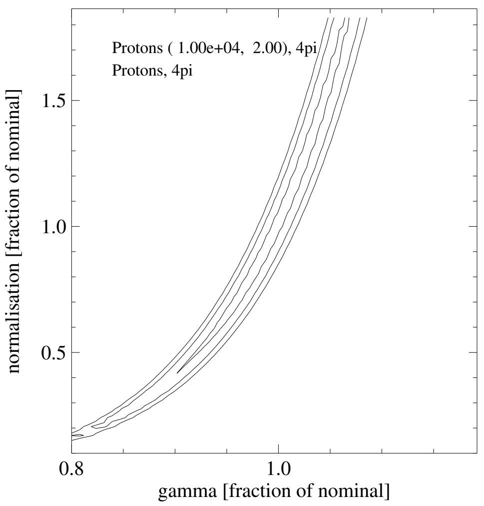

b)

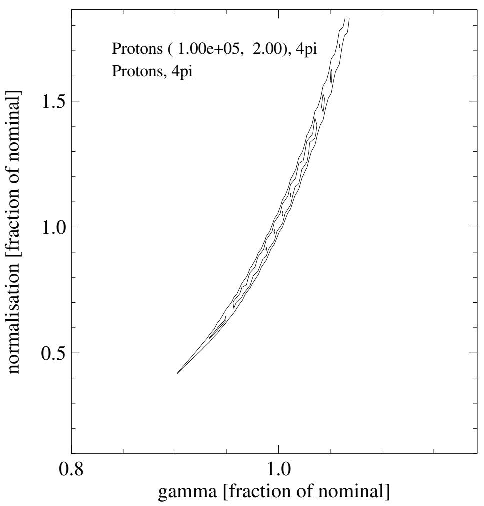

c)

Figure 6: χ^2 as function of the normalization and spectral index γ for protons with power law spectrum. The different panels correspond to measurements with different number of total counts a) 10^3, b) 10^4, and c) 10^5.

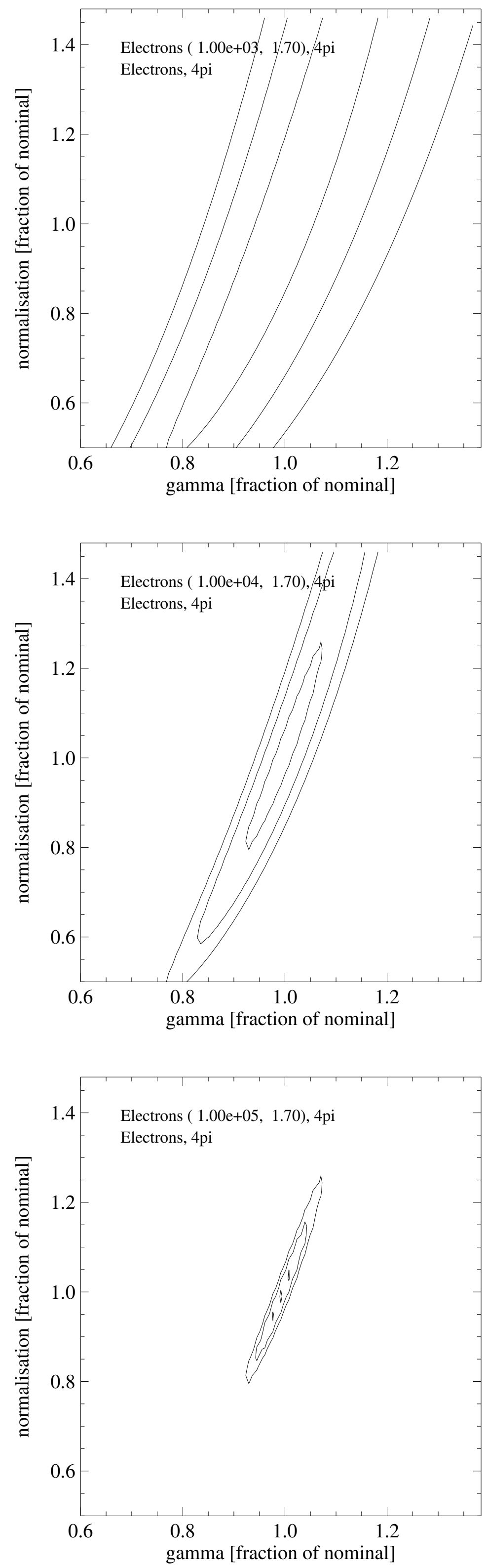

a)

b)

c)

Figure 7: Same as figure 6 but for electrons with exponential spectrum.

$f_p(E_0)$ as spectral parameter ($f_p(E) = f_p(E_0) \cdot E_0^{\gamma} \cdot E^{-\gamma}$). Calculations of χ^2 as function of $f_p(E_0)$ and γ are shown in Appendix B.

- For electrons the spectral index and normalization are similarly well defined, $\pm 10\%$ at 10^4 counts.

3.3.3 Proton-electron resolving power

The same method can also be used to investigate the power of SREM to separate electrons from protons. Therefor the initial count histogram is calculated with one kind of particles and then compared with histograms calculated with the other kind of particles.

Again first only the spectral index was varied and the normalization was selected to keep the total number of counts constant. The results are shown in figure 8 a) initial protons, b) initial electrons. The two lines represent results for number of total counts of 10^3 and 10^4. Note, that in this case χ^2 increases with increasing number of detected particles. Already at 10^4 counts, χ^2 is very large, indicating a good separation of protons and electrons.

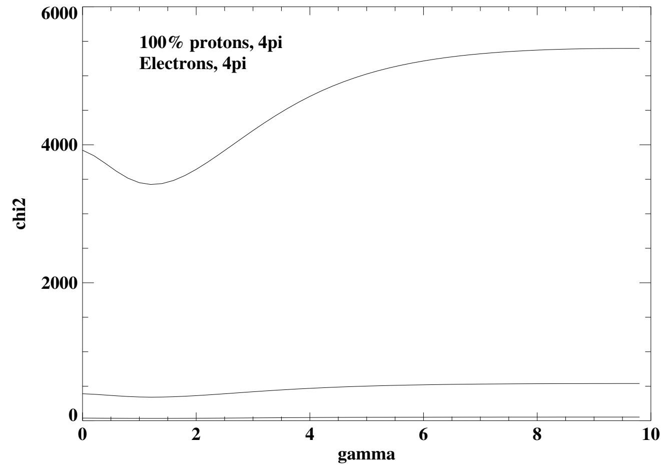

a)

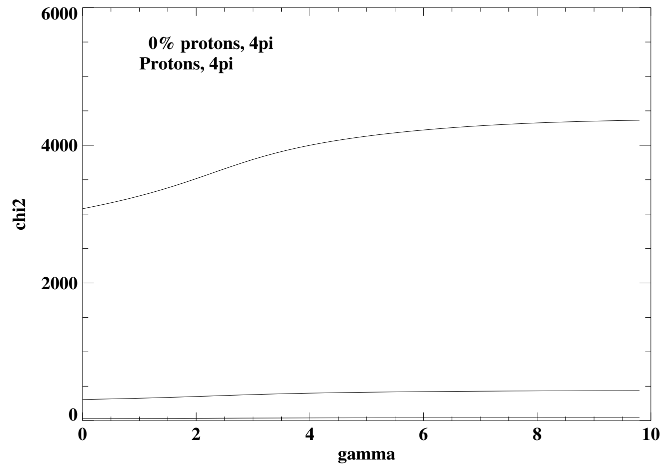

b)

Figure 8: χ^2 as function of the spectral index. a) incident proton spectrum fitted by electron spectrum, b) incident electron spectrum fitted by proton spectrum.

3.4 Spatial information

The SREM is not designed for high-resolution angular measurements. However, with its narrow aperture ($\pm 20°$) and the build in coincidence electronics it should be possible, at least for protons to separate the particles with angles of incidence within the aperture from those arriving from outside the aperture.

For electrons the mass of the SREM box provides sufficient shielding to restrict detections to particles with small angles of incidence. On the other hand protons penetrate from all sides (see figure 1).

3.4.1 Spatial resolving power

To test whether particles arriving from within and outside the aperture can be separated the same method is used which we applied to study the spectral resolving power. The "measured" histogram is computed with particles with $\varphi < \varphi_0$ and is compared, using χ^2 with histograms calculated with particles with $\varphi > \varphi_0$. Results for $\varphi_0 = 20°$ are shown in figure 9 a) protons and b) electrons and for $\varphi_0 = 40°$ in figure 10. The three lines per panel show results for different number of counts (b.t.t.) 10^3, 10^4, and 10^5.

The spectral index of the initial protons with $\varphi < 20°$ is γ_p=2. The best fitting spectrum from the back is much softer, $\gamma \approx 3.4$. The proton spectrum from the front is mimiced by a much softer proton spectrum from the back! Nevertheless, for measurements with more than 10^4 counts, separation of protons from front and back could be feasible.

For electrons χ^2 is significantly smaller, thus separation from front and back particles is less pronounced.

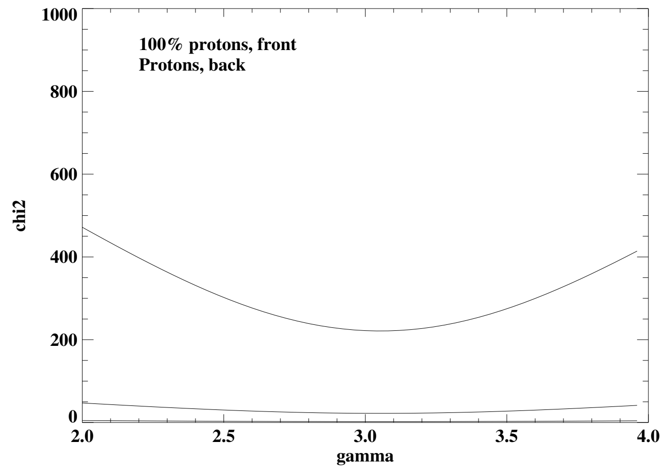

a)

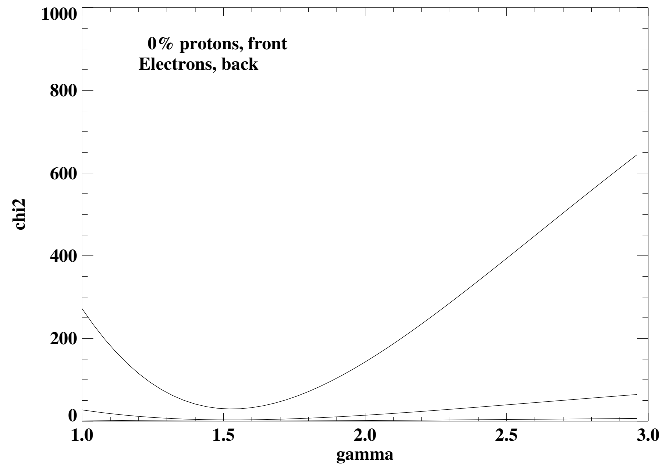

b)

Figure 9: χ^2 computed with spectra from front ($\varphi < 20°$) and back ($\varphi > 20°$) a) protons, b) electrons. The three lines show results for different total number of counts (b.t.t.) 10^3, 10^4, and 10^5.

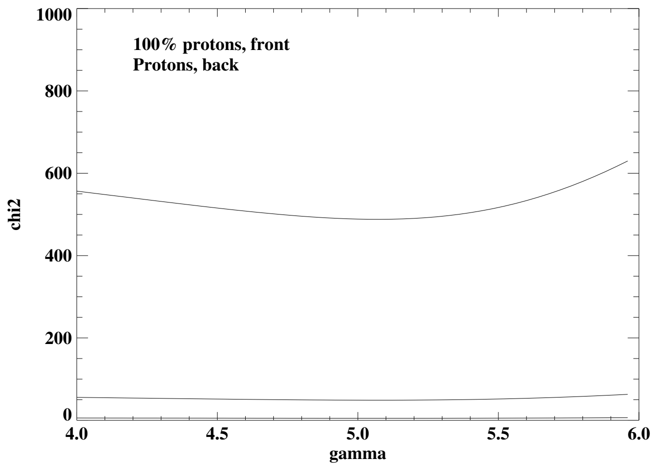

a)

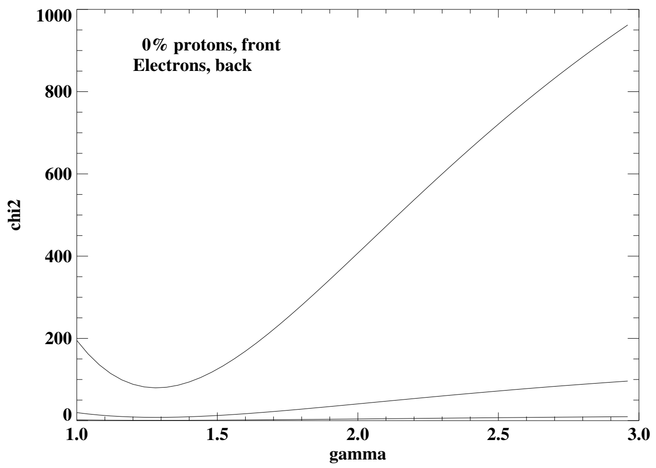

b)

Figure 10: Same as figure 9 but with $\varphi_0 = 40°$.

3.5 Unfolding procedures

Equation (7) has no unique solution since a finite number of discrete measurements cannot define a continuous function. In any case the seeked spectra have to be parametrized in some way. There are two principle possibilities: either the spectra are approximated by a continuous function with a few free parameters or the spectrum is discretized. In the case of the continuous approximation the best fitting parameters are found by minimizing χ^2 (equation (8)). In the case of the discrete approximation, the set of equations (7) is transformed into a linear matrix equation, which can be solved with special algorithms.

3.5.1 Continuous spectral models

Using continuous spectral models to describe the particle spectra, standard fitting algorithms can be used to deduce the best fitting parameters. Many algorithms exist and are available as subroutines for different programming languages. However, good routines must deliver besides the best fitting parameter values also an estimate of the parameter uncertainty. We assume these programs to be ready for use and do not discuss them here any further. For more information we refer to the MINUIT reference manual [*James,* 1994] and references therein.

In order to keep the number of fitting parameters small the spectral models must be simple. Suitable models are listed in table 4.

Table 4: Continuous models for proton and electron differential energy spectra.

name	definition	remarks
power law	$A \cdot E^{\gamma}$	fits well AP8, inner belt
exponential	$A \cdot exp(E \cdot \gamma)$	fits well AE8, outer belt
maxwellian		
kappa	$A \cdot (1 + \alpha \cdot v^2)^{\beta}$	v is the particles velocity

3.5.2 Discrete spectral models

The integral equations can be transformed at least approximatively, into a linear matrix equation by using a step like function to approximate the particle spectra.

$$\begin{aligned} c_i &= \int_0^{\infty} f(E) \cdot G(E,i) dE \\ &= \sum_l \int_{E_l}^{E_{l+1}} f(E) \cdot G(E,i) dE \\ &= \sum_l f(E_l^*) \cdot \int_{E_l}^{E_{l+1}} G(E,i) dE \\ &= \sum_l f(E_l^*) \cdot \mathcal{A}_{l,i} \end{aligned} \tag{9}$$

There has been no approximation until now. There exist energies E_l^* with $E_l \leq E_l^* \leq E_{l+1}$ for which this developement is strictly correct. However, the values of E_l^* depend on the particle spectrum and can not be determined without the full spectral information.

The matrix equation (9) can be used to determine $f(E_l^*)$. $\mathcal{A}$ is a $L \times I$ matrix, where L is the number of energy bins (l=1 .. L) and I is the number of detector counters. The matrix elements $\mathcal{A}_{l,i}$ are defined as

$$\mathcal{A}_{l,i} = \int_{E_l}^{E_{l+1}} G(E,i)dE \tag{10}$$

In the case where $L = I$ the equation can be inverted (assuming rank $\mathcal{A} = I = L$). In the case where $L < I$ the system is overdetermined and the solution has to be found by an optimization procedure. If $L > I$ the system is underdetermined. In this case the available information, the number of counts in I counters, is not sufficient to determine the L flux levels. However, there exist algorithms to find the best fitting spectra under certain assumptions also in this case.

Conversion methods for equation (9) must provide two things: in order to be physically meaningful the solutions must be positive and they must provide error estimates. For detailed information we refer to [*Lawson and Richard,* 1974, *Eadie et al.,* 1982, *Matzke,* 1997, *Höcker and Kartvelishvili,* 1995, *Lucy,* 1974, *Zhigunov,* 1983, *Gagunashvili,* 1983, *Tichy,* 1988]. A similar problem is encountered in neutron dosimetry, where the neutron flux is measured with a system of so called Bonner spheres [*Alevra et al.,* 1988, *Matzke,* 1988]. A software package for solving the underdetermined system in this problem has been developed by Manfred Matzke from the Physikalisch Technische Bundesanstalt in Braunschweig, Germany [*Matzke,* 1994]. The source code was kindly provided to PSI by M. Matzke for further use.

3.5.3 Energy bins

The energy intervals (E_l) can be freely selected. But in order to keep the system overdetermined, which promises to give the most reliable results the number of intervals should not exceed the number of complementary counters. In section 2.2 we noted that the number of complementary proton counters is > 6 and the number of complementary electron counters, ≈ 4.

As an example the proton energy range of 8 to 300 MeV is split into 6, in logarithmic scale, equally spaced intervals and the electron energy range of 0.5 to 6 MeV, into 3 intervals and the energy response for each energy interval is calculated. The results are shown in figures 11 (protons) and 12 (electrons). The left plot in each panel shows the number of counts in each counter. The rigth plot shows the difference between the contribution of particles with angle of incidence $\varphi < 20°$ and particles with $\varphi > 20°$. The total number of detections in each histogram is 10^5.

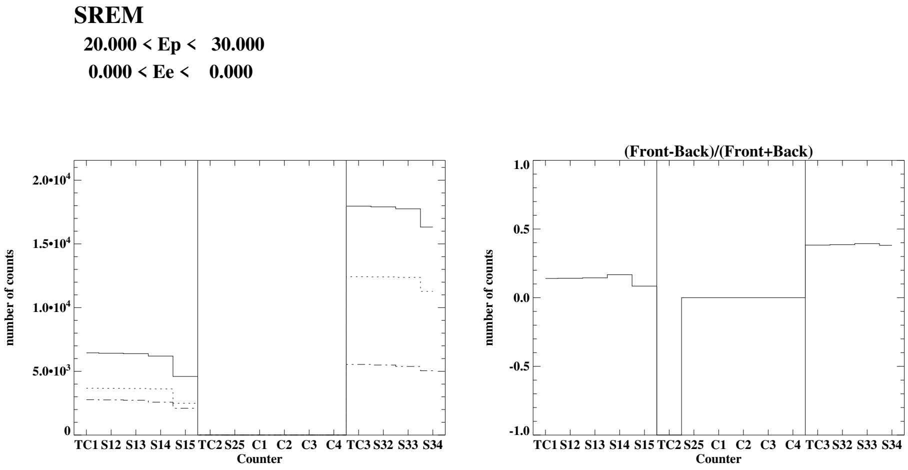

a)

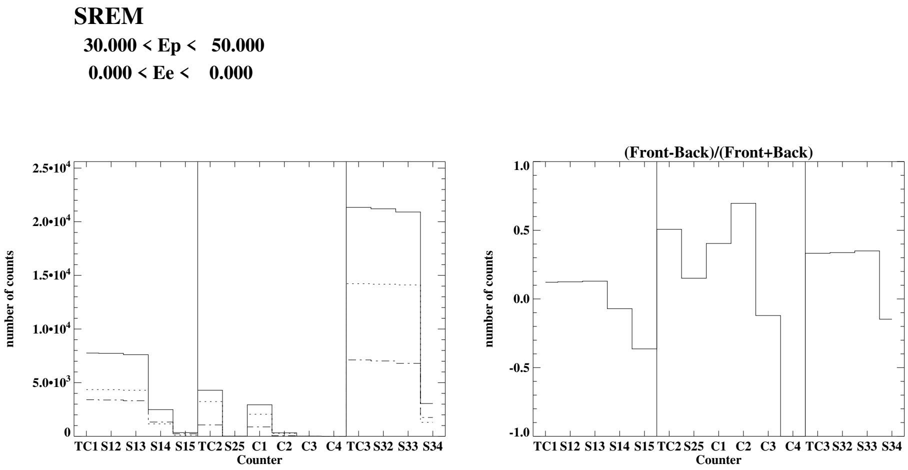

b)

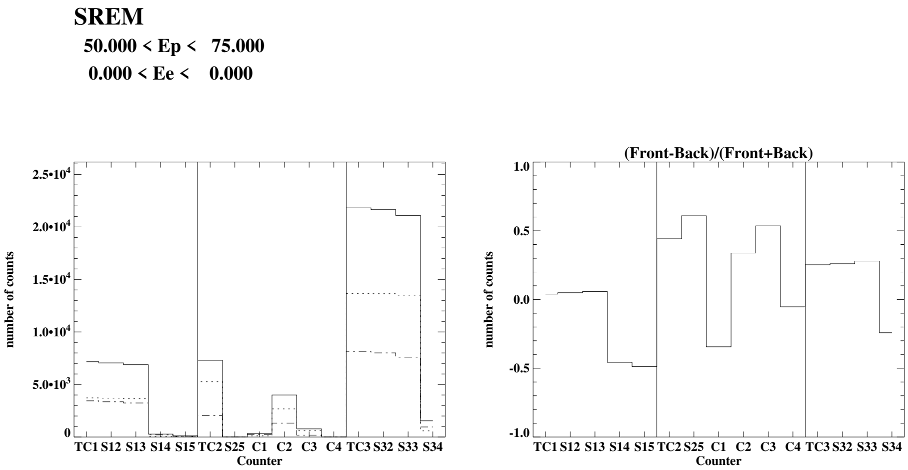

c)

figure 11 continued on next page

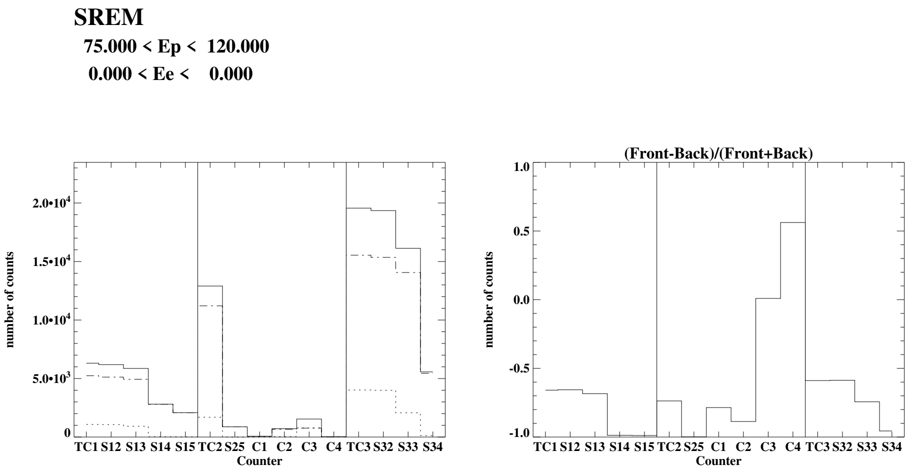

d)

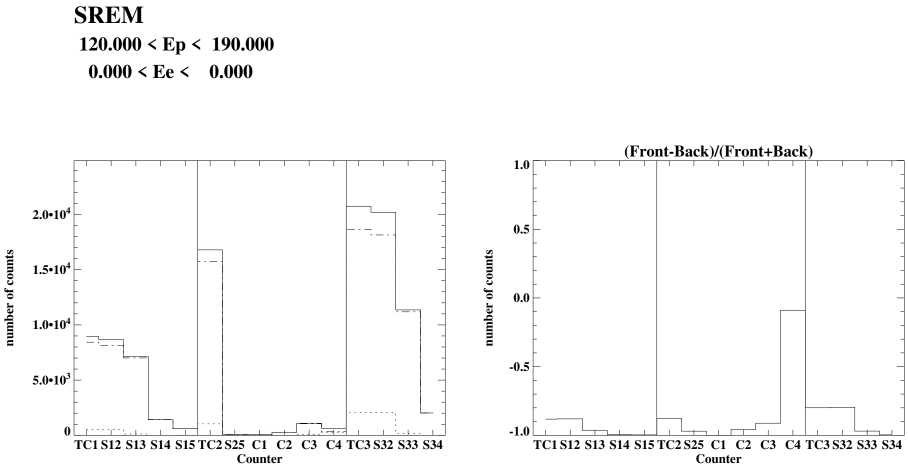

e)

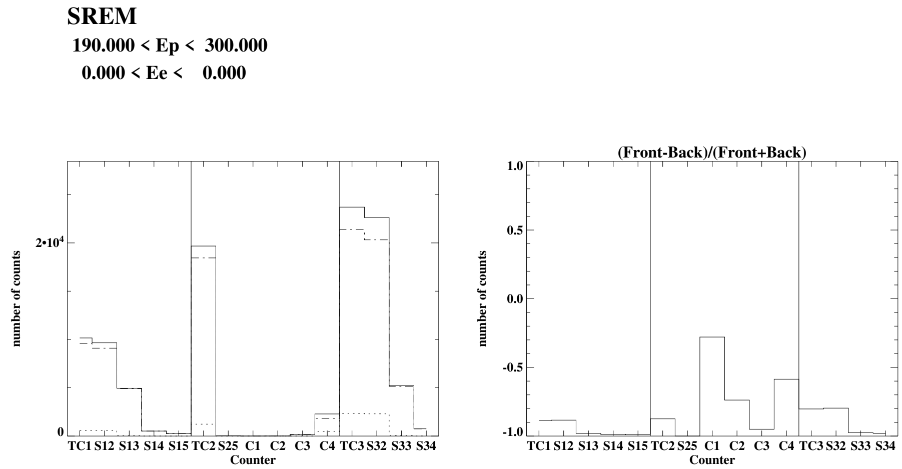

f)

Figure 11: Count histograms (left panels) and (right panels) relative difference between detections from within (dotted line in left panels) and outside (dashed-dotted line in left panels) the aperture of $\pm 20°$ for different proton energy bins a) 20 - 30 MeV b) 30 - 50 MeV c) 50 - 75 MeV d) 75 - 120 MeV e) 120 - 190 MeV f) 190 - 300 MeV.

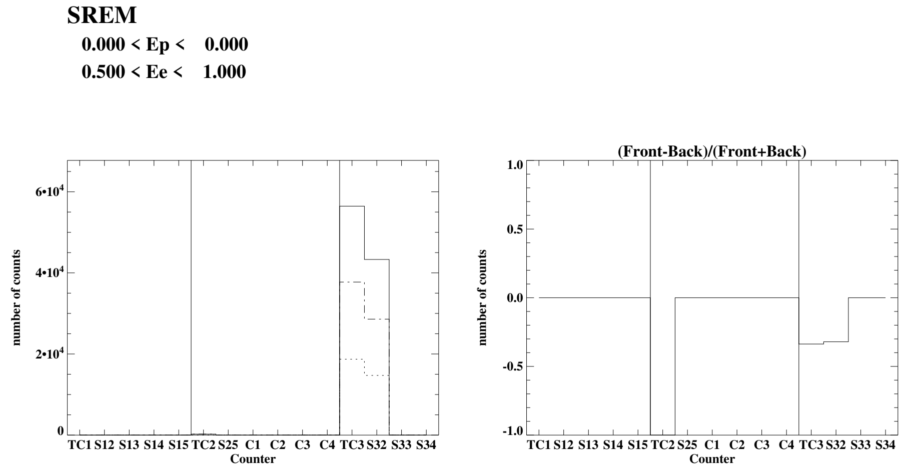

a)

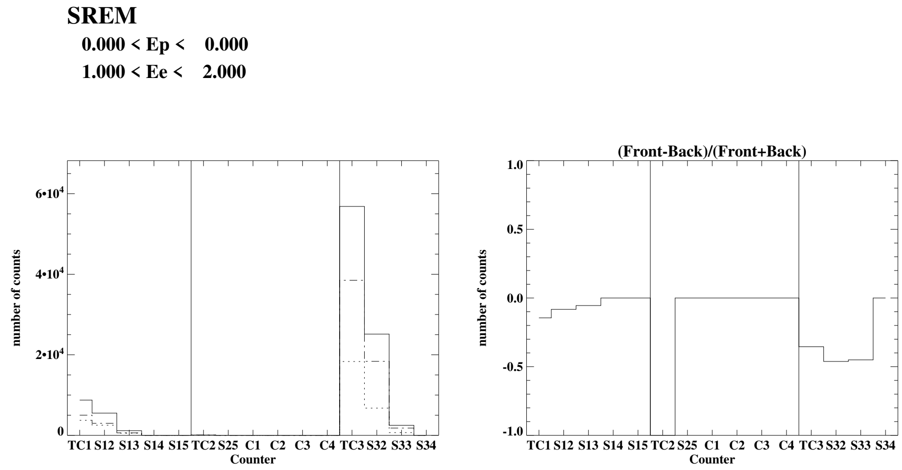

b)

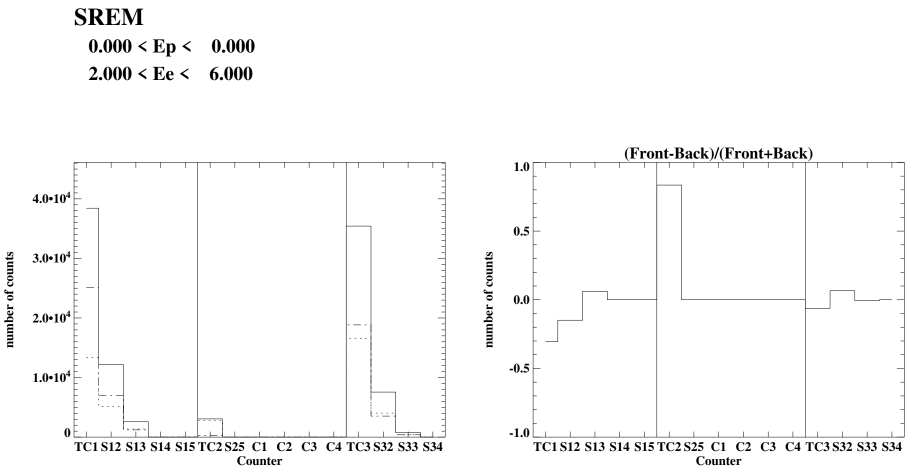

c)

Figure 12: Same as figure 11 but for electron energy bins a) 0.5 - 1.0 MeV b) 1.0 - 2.0 MeV c) 2.0 - 6.0 MeV.

As a measure for the difference between the various histograms again χ^2 can be used. The higher χ^2 is, the better the two energy intervals are resolved. The χ^2-values shown in table 5 have been calculated using flat particle spectra. Only the spectral amplitudes have been varied to minimize χ^2. In all cases the reference histograms contain 10^5 counts.

Table 5: χ^2-values for different proton and electron energy bins at 10^5 counts.

Proton energy range [MeV]		χ^2_{min}	Electron energy range [MeV]		χ^2_{min}
bin 1	bin 2		bin 1	bin 2	
20 - 30	30 - 50	1478	0.5 - 1.0	1.0 - 2.0	1518
20 - 30	50 - 75	2198	0.5 - 1.0	2.0 - 6.0	5398
20 - 30	75 - 120	1579	1.0 - 2.0	2.0 - 6.0	2549
20 - 30	120 - 190	2468			
20 - 30	190 - 300	3332			
30 - 50	50 - 75	607			
30 - 50	75 - 120	849			
30 - 50	120 - 190	1016			
30 - 50	190 - 300	1843			
50 - 75	75 - 120	819			
50 - 75	120 - 190	814			
50 - 75	190 - 300	1518			
75 - 120	120 - 190	447			
75 - 120	190 - 300	1319			
120 - 190	190 - 300	425			

4 Requirements for simulations

Simulations of the SREM detector system are needed to determine its energy response, the geometric factors as function of energy. In order to get the best results, the simulations are performed in two steps. The first step aims to optimize the computer model of the detector geometry and mass distribution. Simulations are performed which can be compared with calibration measurements at PIF [*Hajdas et al.*, 1996] or with radioactive sources (^{60}Co, ^{90}Sr) [*Hajdas*, 1997] which are performed at PSI. After optimization of the model, the mass model of the satellite is added and the final simulations are performed aiming to define the energy response of the onboard detector system.

The presented analysis confirmed the design goals [*Nieminen*, 1995]:

- SREM is sensitive to spectral proton/electron changes
- SREM can separate electrons and protons
- SREM can separate protons from front and protons from back

This implies the following requirements for the simulations.

- Simulations of electrons over full energy range from 4π
- Simulations of protons over full energy range from front ($\varphi < \varphi_0^\circ$)
- Simulations of protons over full energy range from back ($\varphi > \varphi_0^\circ$)

The value of φ_0 must be selected. It will be around 20 to 50°. The final value should be selected by making plots like the ones shown in figure 9 with 4π-simulations including the spacecraft for different φ values. It must be discussed whether geometric factors of electrons from front and back are needed. This would need an additional full set of simulations which especially for electrons is rather time consuming. It is however doubtful if this information can be used to resolve the electron spatial distribution.

The final simulations are performed at a series of fixed energies E_s^k which gives the geometric factors $G_k(E_s^k, i)$. The energies must be selected such that $G_k(E, i)$ can be interpolated with reasonable accuracy for any given energy. The number of simulated particles per energy $N(E_s^k)$ must be sufficient to keep the statistical errors for all detector counters below 10%.

The statistical error ΔG is given by

$$\begin{aligned} \Delta G &= G\sqrt{(\frac{\Delta c_i}{c_i})^2 + \frac{\Delta N}{N})^2} \\ &= G\sqrt{\frac{1}{c_i} + \frac{1}{N}} \\ &\approx G\sqrt{\frac{1}{c_i}} \end{aligned} \tag{11}$$

Thus c_i should be at least 100. However, in cases where $G_k(E, i)$ is very small, e.g. electrons in TC2, this goal will probably not be achieved in reasonable time.

4.1 Simulations, step by step

The following steps are needed to optimize the outcome of the SREM simulations

1. Simulate SREM box from 4π and use results to make first analysis of SREM performance (summarized in this document)
2. Simulate calibrations (PIF, radioactive sources). Compare simulations with measurements to optimize SREM model (ongoing work)
3. Add satellite mass model and make 4π simulations. Use these simulations to repeat the SREM performance analysis and to fix the open parameters (E_s, φ_0, electron/protons - front/back)
4. Perform the final simulations with the required statistical accuracy

A Simulation of an isotropic particle flux

A.1 Isotropy

Let us assume that we have a detector in a radiation field, and that the detector counts the number of particles which penetrate a surface of 1 cm^2 perpendicularly, from one side. If the radiation field is isotropic then the counted number N is independent of the orientation of the detector.

A.2 Simulation

In order to simulate an isotropic particle flux impinging on SREM, the following steps are performed (see figure 1).

1. Selection of Θ and ϕ (direction of incidence)
   This defines point P.
2. Selection of point B in area A.
   A is a circular surface with a radius r_a (the size of the area is $F_A = 4\pi r_A^2$). It stands perpendicular to the line l connecting P and the center of the detector C. R_A denotes the distance between P and C.
3. The particle is submitted from B, parallel to l in the direction of the detector.
4. This procedure is repeated N_{tot} times.

In order to avoid clustering of the selected starting points P at the poles of the sphere with radius R_A, Θ and ϕ are calculated using

$$\begin{aligned} \Theta - \pi/2 &= asin(2\rho_1 - 1) \\ \phi &= 2\pi\rho_2 \qquad (12) \end{aligned}$$
$$(13)$$

where ρ_i are uniformly distributed random numbers with $\rho_i[0, 1]$.

In order to guarantee a homogeneous distribution of the points B in the area A, B_x and B_y are calculated using

$$\begin{aligned} B_x &= r \cdot cos(\alpha) \\ B_y &= r \cdot sin(\alpha) \qquad (14) \end{aligned}$$
$$(15)$$

with

$$\begin{aligned} \alpha &= 2\pi\rho_3 \\ r &= r_A\sqrt{\rho_4} \qquad (16) \end{aligned}$$
$$(17)$$

Again ρ_i are uniformly distributed random numbers with $\rho_i[0, 1]$

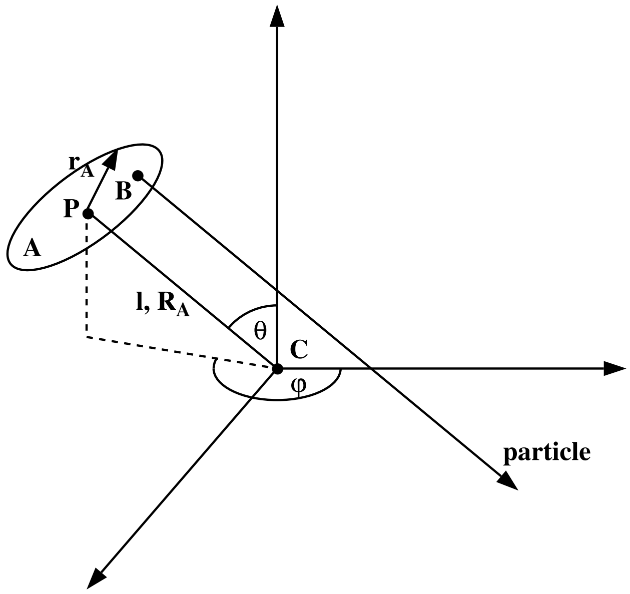

Figure 13: Simulation of an isotropic particle flux.

A.3 Particle flux

Given the described procedure and the total number of simulated particles N_{tot} we can calculate the number of particles N the hypothetical detector described above, located in C, would measure.

$$N = N_{tot}/4\pi/F_A\ [cm^{-2}sr^{-1}] \tag{18}$$

We note that the applied procedure guarantees that this number is independent of the orientation of the detector in space (within the statistical limits of the restricted sample of simulated particles), thus an isotropic flux. The number depends on the size of A but not on the distance R_A.

With N the 4π-flux $F_{4\pi}$ can be calculated with

$$\begin{aligned} F_{4\pi} &= 2\pi \cdot \int_{-\pi}^{\pi} N \cdot cos(\Theta)d\Theta \\ &= 4\pi \cdot N \\ &= N_{tot}/F_A\ [cm^{-2}] \end{aligned} \tag{19}$$

B χ^2 as function of $f_p(E_0)$ and γ

Instead of using normalisation A, which is the flux at 1 MeV, to parametrize the proton spectra one can also use the flux at a given energy E_0. In figure 14 χ^2 is shown as function of $f_p(50MeV)$ and γ for protons. The three panels represent results for different numbers of total counts in the reference histogram (a) - c): 10^3, 10^4, and 10^5).

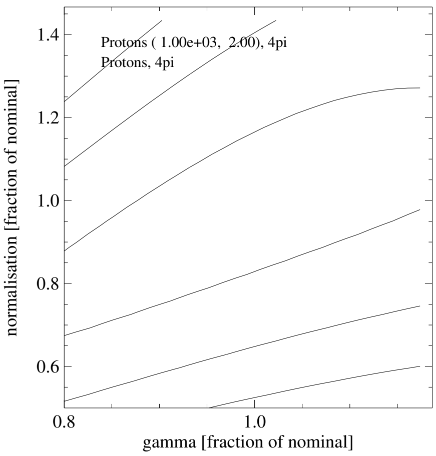

a)

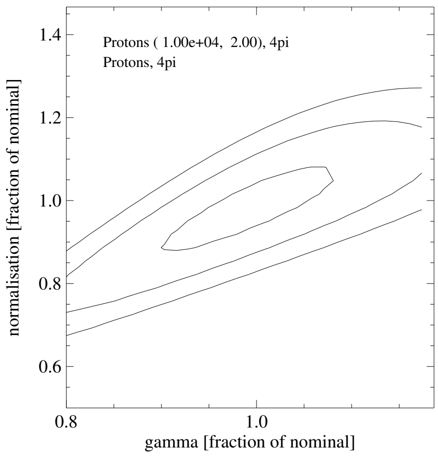

b)

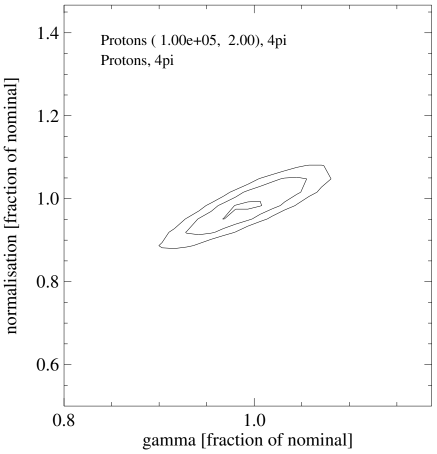

c)

Figure 14: χ^2 as function of the normalization at 50 MeV and spectral index γ for protons with power law spectrum. The different panels represent measurements with different number of total counts a) 10^3, b) 10^4, and c) 10^5.

References

[*Alevra et al.,* 1988] Alevra, A.V., Cosack, M., Hunt, J.B., Thomas, D.J., and Schraube, H., Experimental determination of the response of four bonner sphere sets to monoenergetic neutrons, *Rad. Prot. Dosimetry, 23,* 14, 293, 1988.

[*Cash,* 1976] Cash, W., Generation of confidence intervals for model parameters in X-ray astronomy, *Astron. Astrophys., 53,* 307, 1976.

[*Cash,* 1979] Cash, W., Parameter estimation in astronomy through application of the likelihood ratio, *Astrophys. J., 228,* 939, 1979.

[*Eadie et al.,* 1982] Eadie, W.T., Drijard, D., James, F.E., Roos, M., Sadoulet, B., Statistical methods in experimental physics, North-Holland Publishing Co., New York, USA, 1982.

[*Gagunashvili,* 1983] Gagunashvili, N.D., Unfolding of true distributions from experimental data distorted by detectors with finite resolutions,

[*Hajdas et al.,* 1996] Hajdas, W., Mchedlishvili, A., Schlumpf, N., Zehnder, A., Calibration of Standard Radiation Environment Monitor SREM EM at PSI Proton Irradiation Facility PIF, *PSI internal report,* 1996.

[*Hajdas,* 1997] Hajdas, W., Simulations of the SREM detector box, *PSI internal report,* 1997.

[*Höcker and Kartvelishvili,* 1995] Höcker, A. and Kartvelishvili, V., SVD approach to data unfolding, *CERN preprint,* MC-TH-9515, 1995.

[*James,* 1994] James, F., MINUIT, Function minimization and error analysis, Reference Manual, *CERN Program Library Long Writeup D506,* 1994.

[*Lawson and Richard,* 1974] Lawson, L.L and Richard, J.H., Solving least squares problems, Prentice-Hall Inc., Englewood Cliffs, New Jersey, USA, 1974.

[*Lucy,* 1974] Lucy, L.B., An iterative technique for the rectification of observed distributions, *The Astronomical J., 79,* 6, 745, 1974.

[*Matzke,* 1988] Matzke, M., Estimation of dose equivalents from reaction rates of bonner spheres without using a priori fluence information, *Rad. Prot. Dosimetry, 23,* 14, 297, 1988.

[*Matzke,* 1994] Matzke, M., Unfolding of pulse height spectra: The HEPRO program system, *PTB-report, PTB-N-19,* 1994.

[*Matzke,* 1997] Matzke, M., Unfolding of particle spectra, *Int. Conf.: Neutrons in research and industry, SPIE 2867,* 598, 1997.

[*Nieminen,* 1995] Nieminen, P., Standard Radiation Environment Monitor detector design and simulation, *E.W.P. 1892, ESA/ESTEC*, April 1995.

[*Tichy,* 1988] Tychi, M., Bayesian approach to neutron spectrum adjustment, *Nucl. Instr. Meth. Phys. Res. A, 267,* 502, 1988.

[*Vuilleumier,* 1997] Vuilleumier, P., Standard Radiation Environment Monitor (SREM), Requirements Specification, *ESA/ESTEC internal report, SREM/RS/002,* 1997.

[*Zhigunov,* 1983] Zhigunov, V.P., Improvement of resolution functions as an inverse problem, *Nucl. Instr. Meth., 216,* 183, 1983. *Nucl. Instr. Meth. Phys. Res. A, 343,* 606, 1994.